Friction and wear in surface micromachined tribological test devices*

Donna Cowell Senft and Michael T. Dugger

Sandia National Laboratories, P.O. Box 5800, MS 0340, Albuquerque, NM 87185-0340*

ABSTRACT

We report on the design, construction, and initial testing of surface micromachined devices for the measurement of friction and wear. The devices measure friction coefficients on both horizontal deposited polysilicon surfaces and vertical etched polysilicon surfaces. The contact geometry of the rubbing surfaces is well-defined, and a method is presented for the determination of the normal and frictional forces. Initial observations on test devices which have been dried with supercritical CO_2 and devices coated with octadecyltrichlorosilane (ODTS) suggest that the coatings increase the lifetime of the devices and the repeatability of the results.

Keywords: MEMS, surface micromachined, tribology, friction, wear

1. Introduction

Friction and wear are present in most microelectromechanical systems (MEMS) involving actuators. An understanding of friction and wear in MEMS is necessary to improving the performance and reliability of these devices. Frictional forces are more important in MEMS than for macroscopic moving parts since they have a large surface area to volume ratio. Further, methods of fabrication limit the number of different materials available so that most often contact occurs between self-mated materials which is tribologically detrimental. Existing models of friction and wear rely on the probabilistic interaction of large numbers of asperities. For surface micromachined elements which operate under low loads and have small areas, members may be supported by a single asperity contact. Measurements of friction and wear are needed to develop models to predict device performance.

Although important to the development of surface micromachined devices, little work has been done to characterize friction and wear using micromachined devices where MEMS-scale forces can be applied and measured. Some information has been collected from studying the dynamic behavior of rotating micromachined gears.[1,2] These measurements give a good indication of the friction for a particular device, but since the contact geometries and pressures are unknown, the results cannot be generalized. Other efforts have focused on constructing micromachined devices primarily for the measurement of static friction.[3,4]

Coupling agent coatings are being used to prevent stiction in surface micromachined (SMM) devices[5]. One of the authors[6] has previously shown that the friction force is reduced by coatings of octadecyltrichlorosilane (ODTS). Experiments with untreated and ODTS-treated polysilicon surfaces were done with a pin-on-disk tribometer and showed that untreated surfaces exhibit a rapid increase in the friction coefficient to 0.5 with stick-slip phenomena present. Surfaces treated with ODTS have an initial coefficient of friction of 0.05 which is maintained with reduced stick-slip until the coating is removed or degraded.

This paper describes the design for two types of surface micromachined tribological test devices and initial experimental results from one test device. Our aim is to obtain fundamental information about the coefficient of friction as a function of the contact pressure, under conditions similar to those found in actual devices. Fabricating our test structures in the same way as MEMS devices ensures that the material properties and chemical and morphological nature of the surfaces will be the same. Using micromachined electrostatic comb drives to translate the structures ensures that forces and velocities will be in the desired range.

---

*This work is supported by the United States Department of Energy under Contract DE-AC04-94AL85000. Sandia is a multiprogram laboratory operated by Sandia Corporation, a Lockheed Martin Company, for the United States Department of Energy.

* Further author information -
D.C.S. (correspondence): Email: dssenft@sandia.gov; Telephone: 505-844-4890; Fax: 505-844-7910
M.T.D.: Email: mtdugge@sandia.gov; Telephone: 505-844-1091

2. Experimental Devices

Since there are mainly two different types of surface morphologies found in MEMS, deposited layers and sidewall surfaces, we have constructed two types of test structures for our experiments: the in-plane device and the sidewall device. The in-plane device rubs two horizontal as-deposited polysilicon surfaces together. In the sidewall device two vertical polysilicon surfaces, one a reactive ion etched (RIE) surface, rub together. These structures are fabricated at the Microelectronics Development Laboratory at Sandia National Laboratories and make use of three structural layers of polysilicon referred to as POLY 1, POLY 2, POLY 3, and one layer of doped polysilicon used for electrical connections referred to as POLY 0 as shown in Fig. 1. For our purposes, POLY 1 and POLY 2 together are used as one individual layer. Further details about the processing are described by Garcia and Sniegowski[7]. Accepted materials constants for the polysilicon created by this process are .155 N/μm^2 for Young's modulus and .23 for Poisson's ratio.[8]

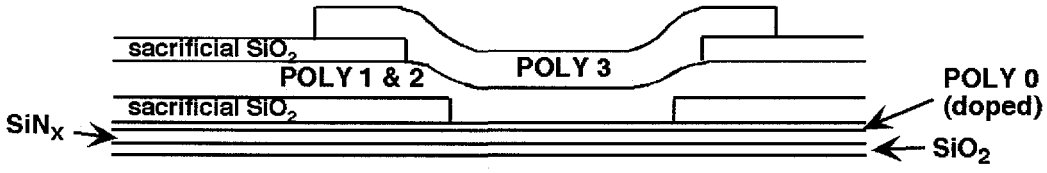

Figure 1 Schematic diagram of the primary layers used in fabricating the tribological test structures.

One of the primary concerns in designing the test structures is the geometry of the flexural elements and contact points. A satisfactory contact geometry is between a sphere and a flat surface. In this case the contact area and pressure can be calculated from the original equations of Hertz. Assuming that the loading force P is known and that the deformation of the surface is entirely elastic, the area of contact is circular with a radius of[9]

$$a = \left[\frac{3\pi P}{16} \frac{(k_1 + k_2)}{(1/R)} \right]^{1/3} \tag{1}$$

where

$$k_i = \frac{1 - \nu_i^2}{E_i}, \quad i = 1,2 \tag{2}$$

ν is Poisson's ratio, R is the radius of the sphere, and E is Young's modulus. The maximum pressure p_0 is given by

$$p_0 = \frac{3P}{2\pi a^2}. \tag{3}$$

In the case of a cylinder contacting a flat surface, the maximum contact stress is given by

$$p_0 = \frac{2P}{\pi a}. \tag{4}$$

The advantage of using a circular contact geometry is that if one of the surfaces becomes tilted due to the movement of the surface, the contact area will remain the same.

The in-plane device shown in Fig. 2(a) uses the sphere-on-flat geometry. The moveable shuttle, which is shown displaced from its equilibrium position in Fig. 2(b), has a rounded bump on the underside. This structure was inspired by static friction test devices fabricated by Lim et al[4]. Electrostatic comb drives to the left and right of the shuttle section can translate the bump back and forth. The electrostatic comb drives are standard actuators used at the Microelectronics Development Laboratory which have integral spring elements and linear comb guides which ensure one-dimensional motion. A pair of folded springs attached to the shuttle give the structure additional stability.

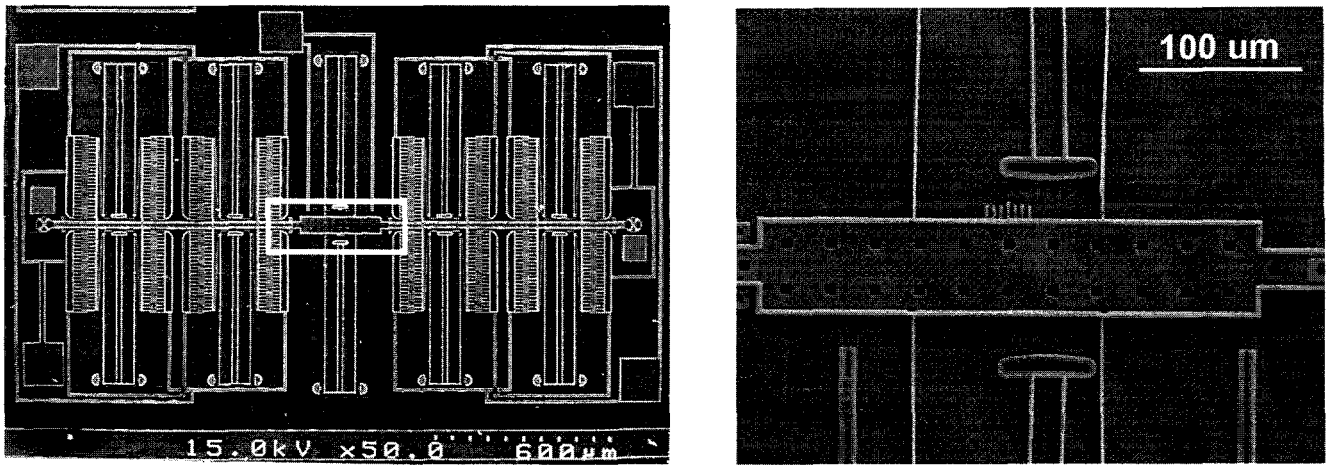

(a) (b)

Figure 2 (a) Layout of the in-plane device showing two electrostatic comb drives with the spring-mounted shuttle in-between. (b) Closeup of the boxed area in (a). Fiducial marks allow the displacement of the shuttle to be read.

The bump on the shuttle is brought into contact with an underlying electrically grounded POLY 0 pad by applying voltages to two additional POLY 0 pads on either side of the ground pad as shown in Fig. 3. A sacrificial silicon dioxide layer separates POLY 0 from the structural polysilicon layers during fabrication. An isotropic etch into the sacrificial layer, creates a rounded mold for the next polysilicon layer, POLY 1. The shuttle itself is made of POLY 1, 2, and 3 and has an overall thickness of 4.5 µm. The width of the shuttle is 60 µm, and the length is 330 µm. The dimensions of the electrostatic contact pads are 80 µm wide by 90 µm long. We have also fabricated wider shuttles with three bumps on the underside giving a larger contact area and greater stability. By considering the shuttle to be an elastic beam and the voltage pads to supply a distributed force load to the beam, the force on the bump can be calculated as a function of the applied voltage. The capacitive force per unit length supplied by the voltage pads, neglecting fringing fields, is given by

$$w = \frac{V^2 \varepsilon_0 b}{2d^2}, \tag{5}$$

where V is the applied voltage, ε_0 is the permittivity of free space, b is the width of the shuttle, and d is the width of the gap between the shuttle and the voltage pad. Assuming that the air gap is equivalent to the height of the bump, 1 µm, and for a shuttle without springs, we can obtain a force of 16 µN by applying 30 V to the voltage pads. Initial testing of this device shows that shuttles without attached springs sometimes tilt, causing one end of the shuttle to come into contact with an electrical pad. This instability has not been observed in shuttles with attached springs.

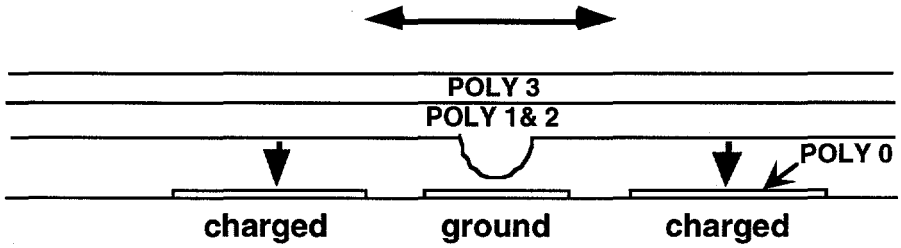

Figure 3 The bump on the underside of the shuttle is electrostatically pulled onto the ground pad. The electrical pads are POLY 0 while the shuttle is made of the three structural layers of polysilicon.

The vertical displacement of the shuttle as the clamping voltage is applied is measured with a Wyko vertical-scanning interferometer with a resolution of 3 nm. With this instrument we can determine the voltage required to bring the bump into contact with the substrate. The interferometer also gives a three-dimensional profile of the shuttle surface which will allow more precise modeling of the deflection of the shuttle as a response to the applied pad voltages. A better model will, in turn, give a better estimate of the force acting on the bump.

The second type of tribological test structure, the sidewall device, is shown in Fig. 4. This device uses the flat-on-cylinder geometry with a 1.8 µm wide by 2.5 µm high rectangular cross-section beam rubbing against a rounded post as seen

in Fig. 4(b). The rounded end of the post has a radius of 2 μm. The beam is fabricated from the POLY 1 and POLY 2 layers. The post is made from the POLY 3 layer. The post has a 4 μm high vertical sidewall with a 2 μm thick cap at the top as shown in Fig. 5. The cap ensures that the beam does not work itself off of the post, although there is a 0.5-1 μm vertical space between the top of the beam and the cap in the equilibrium condition. As fabricated, there is a 2 μm horizontal clearance between the beam and the post. The beam is brought into contact with the post by applying a DC voltage to comb drive 2. Comb drive 1 reciprocates the beam back and forth against the post. Fiducial marks on the elbow of the device can be compared to the fiducial marks on the substrate to determine the position of the device.

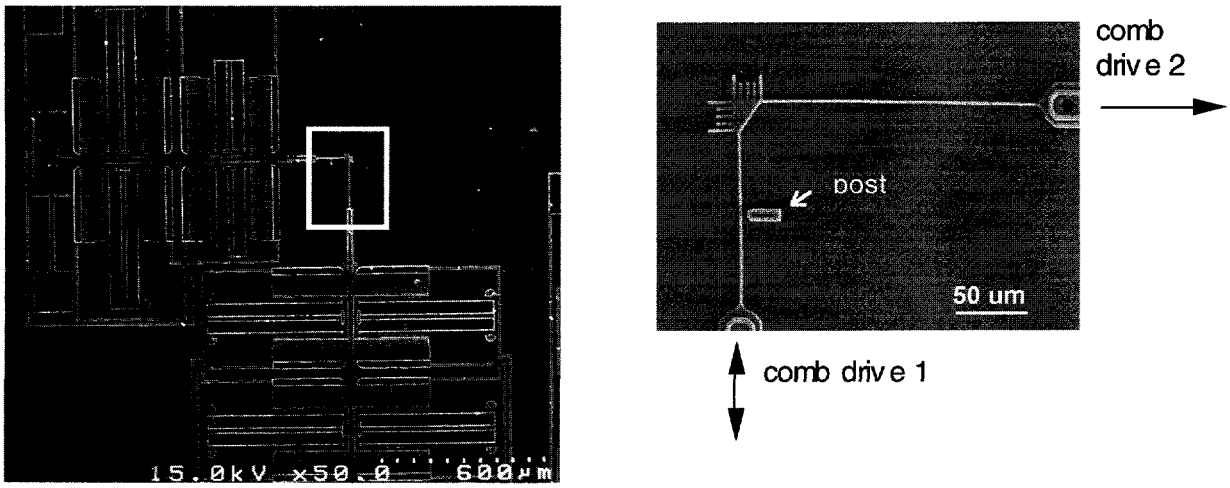

Figure 4 (a) An SEM of the sidewall test device showing the two comb drives at 90° to each other. **(b)** Close-up SEM from the boxed area in (a), showing comb drive 2 which pulls the opposing beam against the post and comb drive 1 which reciprocates the beam back and forth across the post.

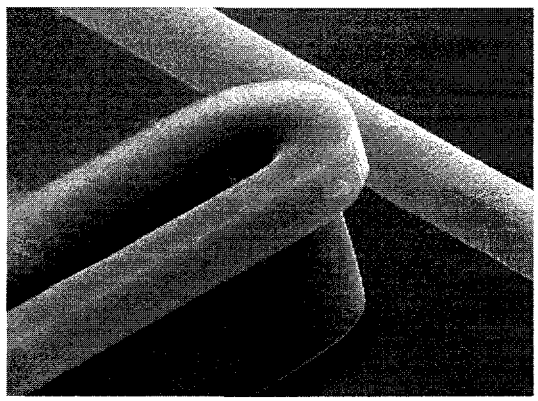

Figure 5 High magnification SEM (6 kX) of contacting elements in the sidewall device. The beam rubs on the lower vertical sidewall of the post, and the cap on the post keeps the beam from sliding off.

3. Experiments

Both devices use comb drives for rubbing the surfaces together. The comb drives are reciprocated by driving them with square waves at frequencies up to 256 Hz. The comb drives have two sets of capacitive fingers; one set is used for pushing and the other set is used for pulling the drive. The drive signals are two square wave signals 180° out of phase. Because the sliding parts have little inertia, the sliding motion in response to the square wave occurs in 0.3 ms or less, after which the parts are stationary for the rest of the half-cycle. The motion of the devices is studied by using strobe light illumination and an image capture system which is triggered in phase with the drive signals and the strobe. An adjustable phase delay between the trigger signal and the drive signals permits examination of all phases of the motion. Later work will concentrate on driving the micromachines with non-simple waveforms at higher frequencies which will move the devices at a constant velocity.

The forces exerted by the comb drives are calibrated by measuring the deflection of a beams as a function of the voltage applied to the comb drive. In the sidewall device comb drive 2 is calibrated by deflecting the beam away from the post to allow a full range of motion. Since the ratio of the width of the yoke of the comb drive to the width of the thin part of the beam is 13:1, the deflection due to the applied force can be considered to occur only in the thin section. Also, the comb drives have guides which prevent rotation of the beams within the comb drive. Then, according to elastic beam theory, the force exerted on the beam is given by

$$P = \frac{3EI\delta}{L^3} = k\,\delta \tag{6}$$

where δ is the deflection of end of the beam (at the fiducial marks), and L is the length of the beam. The variable I is the moment of inertia given by $bh^3/12$ where the base of the beam, b is 2.5 μm, and the height of the beam in the bending direction, h is 1.8 μm.

In the sidewall device the force, F_c exerted by comb drive 1 must overcome the frictional force, f_d of the beam on the post; the force, $k_c\delta$ of the internal drive springs; and the force, $k_b\delta$ exerted by the opposing beam as given by

$$F_c - k_c\delta - f_d - k_b\delta = m\frac{\mathrm{d}^2 x}{\mathrm{d}t^2}. \tag{7}$$

Damping terms due to air resistance are neglected due to the relatively slow frequencies used. Frictional forces internal to the comb drive are absorbed in the other comb drive terms. The force exerted by the comb drives is given by[2]

$$F_c = \frac{n\varepsilon_0 h}{g}V^2 = \pm aV^2 \tag{8}$$

where n is the number of fingers in the comb drive, ε_0 is the permittivity of free space, h is the comb thickness, and g is the gap between the fingers. Each comb drive has two sets of drive fingers, and the direction of the comb drive force depends upon which set of comb drive fingers the voltage is applied. When a voltage is applied to the comb drive initiating an attractive force, the static friction forces are overcome and the comb drive starts accelerating. As the displacement increases, the restoring force due to the internal springs in the comb drive and the deflection of the opposing beam increases. The force due to the dynamic coefficient of friction from the beam on the post is assumed to be constant. The comb drive advances until a force balance is achieved and motion ceases. At this point the deflection of the opposing beam is measured. In a separate measurement when the beam is not in contact with the post, the displacement is measured as a function of the applied voltage, as shown in Fig. 6 and described by the equation

$$F_c = aV^2 = (k_c + k_b)\delta_0. \tag{9}$$

The slope of the curve in Fig. 6, $a/(k_c + k_b)$ is, in this case, $3.1\text{x}10^{-3}$ μm/V^2. Combining this value for the slope, a value of $1\text{x}10^{-7}$ N/μm for δ_b from Eq. (6), and the value of a calculated from Eq. (8), we obtain a value of $8.4\ \text{x}10^{-8}$ N/μm for the value of k_c. To obtain a general expression for the frictional force in terms of measured and calculated values, equations (7) and (9) are combined with the result being

$$f_d = (k_b + k_c)(\delta_0 - \delta). \tag{10}$$

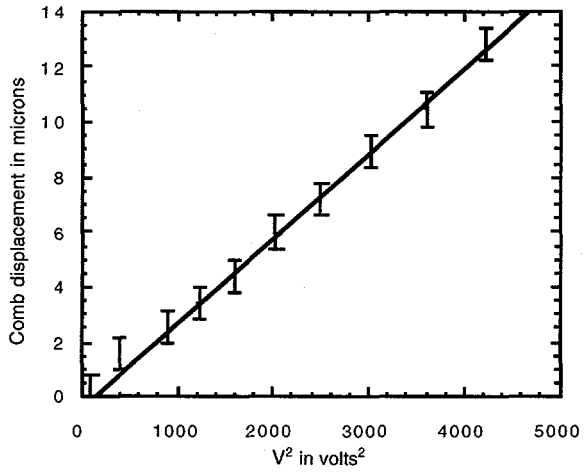

Figure 6 Calibration of comb drive 1 with error bars determined by the pixel size of the captured image.

The normal force between the beam and the post in the sidewall device is equal to twice the force output of comb drive 2 since the comb drive and an equal reaction force both act upon the post. The normal force acting on the post is nearly constant as comb drive 1 is displaced. The force output of comb drive 2 must be calibrated in order to determine the normal force. Since the force output of the comb drive may depend on many variables, such as the region of the wafer where the device originates, the ambient humidity, and the length of time since the wafer was released, the force is calibrated on each device immediately before each experiment. The force vs. the square of the applied voltage is linear after the displacement of the beam exceeds about 2 μm. Sources of error in this calculation are the value of Young's modulus which may change due to process variations, the thickness and width of the beam, and the error in the measurement of the deflection which is primarily caused by the width of the pixel in the captured image (.6 μm at 200X magnification). Since these sources of error should remain constant with experiments on devices from the same wafer, the force measurements will be consistent within a given wafer.

Another source of error in the calculation of the normal force is that when the beam is forced against the post, another part of the beam is forced against the linear comb guide by the reaction force, creating an additional frictional drag. The force on the comb guide is in the opposite direction and with half the magnitude of the normal force. Future designs of the sidewall device will attempt to limit this source of uncertainty.

To prevent stiction from occurring between the moving parts of our devices and the substrate, some of our devices were supercritically dried with CO_2 immediately after the release etch. The devices dried in this manner are entirely free moving, but do have some particle contamination. The other portion of our wafers have an ODTS coating applied which also leaves the devices free moving. After release and drying, all devices are kept in a desiccator to prevent moisture from collecting on surfaces during storage. Tests of the devices are conducted in ambient air.

4. Results

Initial results from experiments with the sidewall device give an estimate for the coefficient of friction for coated and uncoated polysilicon. In the first experiment with an ODTS-coated sidewall device, an 85 V DC signal was applied to comb drive 2 giving a normal force of the beam on the post of 13.5 μN, and a Hertzian contact pressure of 59 MPa. The normal force is determined by measuring the deflection of the beam away from the post in a separate calibration procedure. Comb drive 1 is then reciprocated by applying square wave drive signals with an amplitude of 77 V and a frequency of 32 Hz. During the experiment a video frame showing the position of the device is captured every 96 cycles, usually at a phase of 0° with respect to the comb drive signals, but occasionally at a phase of 180°. Figure 7 is a plot of the device positions measured from these video frames. The positions shown in the video frames taken at 0° and 180° show the maximum deflections of the beam in either direction which gives us δ in Eq. 10 and gives an indication of the force acting on the beam.

The deflection of the beam due to the reciprocation force was constant for the first 80 minutes of the experiment indicating that the friction force was also constant for this period. Thereafter the beam would occasionally stick in the 180° phase position. During these periods it appears that the static friction exceeded the combined attractive force of comb drive 1 and the restoring force of the spring elements. At some later period, perhaps many cycles later, the static friction force would be overcome, and the device would deflect in the opposite direction in response to the driving signals. The occasional

sticking events continued until the device totally ceased movement after at an elapsed time of 140 minutes. The measured displacement of the device in response to the square waves was ± 7.6 μm as compared to a displacement of $\delta_0 = \pm 17.8$ μm when there is no contact between the post and beam. Using these values and equation (10), we obtain a friction force of 1.8 μN and a friction coefficient of 0.14 at one hour after testing started.

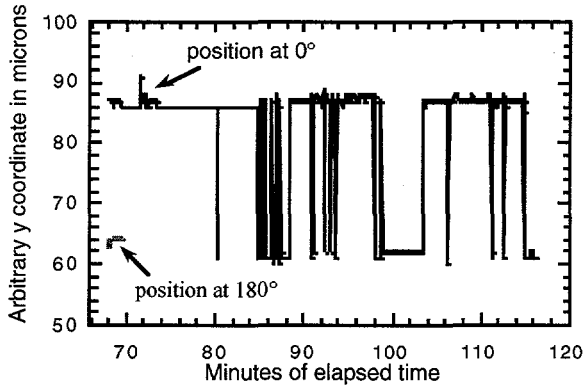

Figure 7 Plot of the coordinates of the position of the sidewall device after 69 minutes of running time and triggered at 0° and 180° phase from the drive signals.

A supercritically-dried sidewall device without the ODTS coating has also been tested with a portion of the results shown in Fig. 8. For this experiment a DC voltage of 80 V was applied to comb drive 2 producing a normal force on the post of 9.8 μN and a Hertzian contact pressure of 48 MPa. A 32 Hz square wave with an amplitude of 77 V was applied to comb drive 1. The amplitude of the motion was $\delta = \pm 8.1$ μm as compared to $\delta_0 = \pm 17.8$ μm for the undamped movement of an unloaded beam. An image showing the position of the device was captured every 15 frames. The position of the device at 0° phase was steady for the first 10 minutes of running time. Thereafter the images showed the same sticking behavior seen in the ODTS-coated device, and the motion of the device stopped completely after approximately 40 minutes. The friction force at the beginning of the run was found to be 1.6 μN which corresponds to an initial friction coefficient of 0.16.

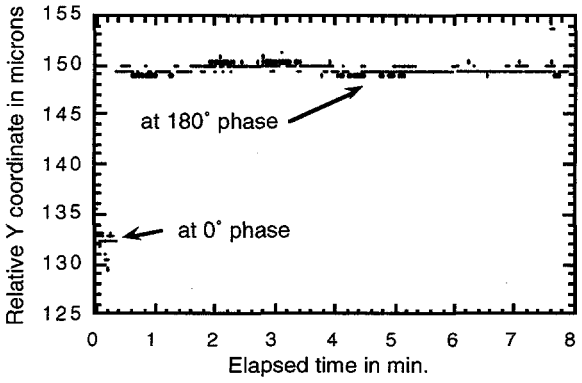

Figure 8 The position of supercritically dried sidewall device at 0° and 180° phase with respect to the drive signals indicates the movement of the device.

After this experiment, the force output of comb drive 2 was calibrated on a sidewall device coated with ODTS. The force output of the coated and uncoated comb drives was identical. The next day the calibrations were repeated with unused ODTS-coated and uncoated devices. This time the force output of the coated device was the same as before, but the maximum output of the uncoated devices were half the previous value. Attempts to repeat the above experiment with uncoated drives were unsuccessful since comb drive 1 would not move against the frictional load. Additional work is needed to determine the repeatability of the friction and wear results.

5. Discussion and Conclusions

We have made initial friction coefficient measurements on polysilicon surfaces for both supercritically dried devices and devices coated with coupling agents. The device coated with ODTS was found to have a lifetime greater than three times the uncoated structure at a contact pressure of 59 MPa as opposed to 48 MPa for the uncoated device, but the friction coefficient was found to be 0.14-0.16 for both surfaces. The measurement error in the coefficient of friction values is estimated to be ± .02. The values obtained for the lifetimes of the devices are based on only a few initial observations and are probably subject to large statistical uncertainties. The value is smaller than the value of 0.50 calculated by Miller et al[2] for the friction coefficient between the rotor and hub of an uncoated SMM microengine. The results for the uncoated device represent the best of the results we obtained, since in other trials the device would not move at all under the same loading force. Stick-slip motion was found to occur for both the coated and uncoated devices but started after a longer rubbing interval in the case of the ODTS-treated surface.

We have demonstrated that is possible to obtain friction information from surface micromachined devices at known contact pressures. The damping force due to friction is determined by the reduction in the amplitude of oscillations of a electrostatic comb drive. Both normal and frictional forces have been determined by measuring the deflection of polysilicon beams. Our future plans are to optimize the designs for the test devices presented in this paper, and to make measurements with the in-plane device as well as more extensive measurements with the sidewall device to fully map out the friction behavior at different contact pressures and velocities. The effect of surface modification on the friction coefficient and wear rates will be measured. The worn surfaces will be examined by atomic force microscopy and other surface analytical techniques in order to detect topographical and chemical changes during wear. The current analysis for the normal and frictional forces depends sensitively on of the width of the beams. Unfortunately, this dimension is not known with a great deal of accuracy at the present time. Some of our future efforts will be devoted to making a more accurate measurement of the beam dimensions or to devising better calibration methods to obtain better estimates of the friction coefficient. Also, the reproducibility of our results with the uncoated, hydrophilic devices would probably be improved by running the experiments in a controlled humidity environment.

ACKNOWLEDGEMENTS

We would like to thank Steven Rodgers for his help in designing our devices and Elizabeth Sorroche, Glenn LaVigne, Norman Smith, and Greg Poulter for their help in assembling the test and analysis system.

REFERENCES

1. K. J. Gabriel, F. Behi., R. Mahadevan, and M. Mehregany, "*In situ* friction and wear measurements in integrated polysilicon mechanisms", Sensors and Actuators **A21-A23,** pp. 184-188, 1990.
2. S. L. Miller, J. J. Sniegowski, G. LaVigne, and P. J. McWhorter, "Friction in surface micromachined microengines", *Proc. SPIE Smart Electronics and MEMS* Vol. 2722, pp. 197-204, San Diego, 1996.
3. R. Prasad, N. MacDonald, and D. Taylor, "Micro-instrumentation for tribological measurement", *Transducers '95 : Proceedings of the 8th International Conference on Solid-State Sensors and Actuators, Eurosensors IX,* p. 244 , Stockholm, 1995.
4. M. G. Lim, J. C. Chang, D. P. Schultz, et al, "Polysilicon microstructures to characterize static friction", *Proceedings of the IEEE Micro Electro Mechanical Systems Workshop*, eds. J. E. Wood & R. T. Howe, pp. 82-88, Napa Valley, California, 1990.
5. R. Maboudian and R. T. Howe, "Adhesion in surface micromechanical structures", J. Vac. Sci. Technol. B **15**, pp. 1-20, 1997.
6. R. R. Rye, G. C. Nelson, and M. T. Dugger, "Surface Chemistry of Alkylchlorosilane Coupling Reactions", Langmuir, **13**, pp. 2965-2972, 1997.
7. E. J. Garcia and J. J. Sniegowski, "Surface micromachined microengine", Sensors and Actuators **A 48**, pp. 203-214, 1995.
8. Sandia National Laboratories SUMMIT design course manual, 1997.
9. N.P. Suh, *Tribophysics*, Chapter 4, Prentice-Hall, Englewood Cliffs, NJ, 1986.

DISCLAIMER